



LAWRENCE  
LIVERMORE  
NATIONAL  
LABORATORY

# Carriers of the astronomical 2175 Å extinction feature

J. Bradley, Z. Dai, R. Ernie, N. Browning, G. Graham,  
P. Weber, J. Smith, I. Hutcheon, H. Ishii, S. Bajt, C.  
Floss, F. Stadermann

August 3, 2004

Science

## **Disclaimer**

---

This document was prepared as an account of work sponsored by an agency of the United States Government. Neither the United States Government nor the University of California nor any of their employees, makes any warranty, express or implied, or assumes any legal liability or responsibility for the accuracy, completeness, or usefulness of any information, apparatus, product, or process disclosed, or represents that its use would not infringe privately owned rights. Reference herein to any specific commercial product, process, or service by trade name, trademark, manufacturer, or otherwise, does not necessarily constitute or imply its endorsement, recommendation, or favoring by the United States Government or the University of California. The views and opinions of authors expressed herein do not necessarily state or reflect those of the United States Government or the University of California, and shall not be used for advertising or product endorsement purposes.

# Carriers of the astronomical 2175 Å extinction feature

**J. Bradley<sup>1</sup>, Z. Dai<sup>1</sup>, R. Ernie<sup>2,3</sup>, N. Browning<sup>2,3</sup>, G. Graham<sup>1</sup>, P. Weber<sup>1</sup>,  
J. Smith<sup>1</sup>, I. Hutcheon<sup>1</sup>, H. Ishii<sup>1</sup>, S. Bajt<sup>1</sup>, C. Floss<sup>4</sup> and F. Stadermann<sup>4</sup>**

**<sup>1</sup>Institute for Geophysics and Planetary Physics, Lawrence Livermore National  
Laboratory Livermore, CA 94550**

**<sup>2</sup>Department of Chemical Engineering, University of California at Davis,  
CA 95616, USA**

**<sup>3</sup>National Center for Electron Microscopy, Lawrence Berkeley National  
Laboratory, CA 94720**

**<sup>4</sup>Laboratory for Space Sciences, Washington University  
St. Louis, MO 63130**

**Submitted to *Nature* July 2004**

**The 2175 Å extinction feature is by far the strongest spectral signature of interstellar dust observed by astronomers. Forty years after its discovery the origin of the feature and the nature of the carrier remain controversial. The feature is enigmatic because although its central wavelength is almost invariant its bandwidth varies strongly from one sightline to another, suggesting multiple carriers or a single carrier with variable properties. Using a monochromated transmission electron microscope and valence electron energy-loss spectroscopy we have detected a 5.7 eV (2175 Å) feature in submicrometer-sized interstellar grains within interplanetary dust particles (IDPs) collected in the stratosphere. The carriers are organic carbon and amorphous silicates that are abundant and closely associated with one another both in IDPs and in the interstellar medium. Multiple carriers rather than a single carrier may explain the invariant central wavelength and variable bandwidth of the astronomical 2175 Å feature.**

Much of what is known about grains in space comes from spectral features observed in reflection, emission, polarization and extinction<sup>1-5</sup>. The strongest feature by far is the so-called “~2175 Å bump” that can be observed in the interstellar medium (ISM) along almost every galactic line of sight (Figs. 1a&b). From interstellar abundances of the elements and known ultraviolet (UV) transitions the carrier is likely either carbon-rich or oxygen-rich, possibly combined with H, Mg, Si, and Fe in various proportions<sup>2,3</sup>. Most astronomers ascribe it to some form of amorphous or graphitic carbon because photon induced electronic ( $\pi \rightarrow \pi^*$ ) transitions in graphite produce a ~2175 Å feature, and the strength of the feature is consistent with the interstellar abundance of carbon<sup>3</sup>. While graphite can explain the constant position it cannot explain variations in bandwidth (full width at half maximum, FWHM) of the feature observed from one line-of-sight to another. This problem appears to be common to most forms of inorganic and organic carbon<sup>3</sup>. Oxygen-based carriers that have been proposed include silicates and oxides containing Mg, Si, Fe, as well as hydroxylated amorphous magnesium silicates<sup>2,6</sup>. The position and the bandwidth of some hydroxylated silicate features match the interstellar feature (Fig. 1c)<sup>6</sup>.

We searched for the ~2175 Å UV feature in chondritic interplanetary dust particles (IDPs) collected in the stratosphere. IDPs are tiny objects, typically <20 µm diameter, composed mostly of aggregates of submicrometer and nanometer-sized grains containing crystalline silicates, sulfides, metal, amorphous silicates, and carbon<sup>7-16</sup>. They are from comets and asteroids and they include the most chemically and isotopically primitive meteoritic materials available for laboratory investigations<sup>12-16</sup>. IDPs are logical materials in which to look for carriers of the 2175 Å feature because estimates of the abundance of preserved interstellar material in IDPs (450-5500 ppm) are 10-100x higher than in the most cosmically primitive class of carbon-rich meteorites, the carbonaceous chondrites<sup>15,16</sup>. Interstellar amorphous silicates and carbon, the two most abundant grain types in the interstellar medium, have been found in chondritic IDPs (Fig. 2). The amorphous silicates are “GEMS” (glass with embedded metal and sulfides) some of which have non-solar O isotopic compositions<sup>16-18</sup>. Some GEMS exhibit a ~10 µm feature that matches the interstellar 9.7 µm “amorphous silicate” feature<sup>18</sup>. The carbon is a mixture of inorganic and organic carbon and some of it exhibits non-solar D/H, <sup>15</sup>N/<sup>14</sup>N, and <sup>13</sup>C/<sup>12</sup>C

ratios of magnitudes comparable to those observed in interstellar molecular clouds<sup>13-15,19-21</sup>.

We used a new generation transmission electron microscope (TEM) equipped with a monochromator and high-resolution electron energy-loss spectrometer to measure UV spectral properties<sup>22</sup>. The region of an electron energy-loss spectrum between 0 and ~100 eV is called the low-loss or valence electron energy-loss spectroscopy (VEELS) region where features due to collective plasma oscillations and single electron transitions of valence electrons are observed<sup>23,24</sup>. We used VEELS to make the measurements because IDPs have proven difficult to measure using conventional UV spectroscopy due to their sub-nanogram masses<sup>25</sup>. The monochromator provides unprecedented access with atomic-scale spatial resolution and detection limits to the 1-10 eV energy (1241-124 nm wavelength) region that includes the 5.7 eV (2175 Å) region. Although the measurements were made using VEELS rather than photo-absorption spectroscopy used by astronomers, the VEELS data were acquired under (electron optical) conditions where the features are directly comparable<sup>26,27</sup>. A synchrotron light source was used to measure infrared (IR) spectral properties<sup>14,18</sup>, and a NanoSIMS ion microprobe to measure the isotopic compositions of the grains within IDPs<sup>28</sup>.

## Observations

Figure 2 shows a brightfield image of carbon and GEMS in a fragment of carbon-rich chondritic IDP L2009\*E2. The bulk composition of the particle is within a factor of two chondritic (solar) for all major elements except C which is ~3X chondritic (solar) abundance<sup>29</sup>. Nearly all the GEMS and other mineral grains in L2009\*E2 are encapsulated in amorphous carbon. Ion microprobe measurements indicate that some of the carbon is of interstellar origin. A bulk  $\delta D$  of 400‰ associated with carbon was measured in L2009\*E2 and related fragments from the same IDP show  $\delta D$  as high as +11,000‰, similar to  $\delta D$  values observed in interstellar molecular clouds<sup>29</sup>.

A VEELS spectrum from an electron-irradiated specimen of the mineral talc ( $Mg_3Si_4O_{10}[OH]_2$ ) is plotted in Figure 1d. Talc rapidly amorphizes under electron irradiation and the strength of the 5.7 eV feature increases with dose. The peak position and bandwidth of the talc feature match the photo-absorption feature of partially recrystallized, hydroxylated magnesium silicate  $Mg_2SiO_4 [OH]_x$  (Figs. 1c & d)<sup>6</sup>. The talc feature also matches the astronomical UV feature (Figs. 1a, b & d). VEELS spectra from carbon grains in three IDPs and an amorphous carbon thin-film standard are plotted in Figure 3a. The carbon in each of the grains exhibits a 5.7 eV feature with an average bandwidth (FWHM) of 2.6 eV ( $2.2 \mu m^{-1}$ ). Amorphous inorganic carbon exhibits a similar feature but at a significantly higher energy (6.3 eV) and volume plasmon position (24.5 eV). There is downward shift in the peak energy of the volume plasmon with increasing strength of the 5.7 eV feature. The 5.7 eV from L2036-C18-F4 is the weakest and the volume plasmon peaks at 24.0 eV, whereas 5.7 eV feature from L2036-G16 is the strongest and the volume plasmon peak is shifted downwards to ~22.7 eV. The strength of the 5.7 eV carbon feature also correlates with the O/C ratio (Fig. 3). Energy-loss C and O core scattering edges from the most O-rich regions exhibit fine structure consistent with carbonyl (or hydroxyl) functional groups (Fig. 4)<sup>20</sup>. Infrared (IR) spectra from the

same regions exhibit prominent C-H stretch and C=O features at  $\sim 3.4 \mu\text{m}$  and a  $5.9 \mu\text{m}$  respectively (Fig. 4). Although signal-to-noise is low, due to extreme thinness of the specimen ( $\sim 100 \text{ nm}$ ), the overall structure of the C-H stretch feature between  $2850$  and  $3100 \text{ cm}^{-1}$  is consistent with aliphatic groups bound to other molecules (most likely PAHs) (Fig. 4)<sup>30,31</sup>. VEELS spectra were obtained from pyrene ( $\text{C}_{16}\text{H}_{10}$ ), 1-pyrene carboxaldehyde ( $\text{C}_{17}\text{H}_{10}\text{O}$ ), pentacene ( $\text{C}_{16}\text{H}_{10}$ ), pentacene quinone ( $\text{C}_{16}\text{H}_{12}\text{O}_2$ ). The PAHs with carbonyl functionality ( $\text{C}_{17}\text{H}_{10}\text{O}$  and  $\text{C}_{16}\text{H}_{12}\text{O}_2$ ) exhibit a  $5.7 \text{ eV}$  feature while the unsubstituted PAHs ( $\text{C}_{16}\text{H}_{10}$  and  $\text{C}_{16}\text{H}_{10}$ ) do not. GEMS produce a  $5.7 \text{ eV}$  feature with an average bandwidth (FWHM) of  $2.9 \text{ eV}$  ( $2.5 \mu\text{m}^{-1}$ ) and the strength of the feature correlates strongly with hydroxyl (OH) abundance expressed as oxygen excess over stoichiometry ( $\text{O}_{\text{ex}}$ ) (Fig. 5)<sup>17</sup>.

The isotopic compositions of several of the carbon and GEMS grains were measured using NanoSIMS ion microprobes. The VEELS spectrum from L2047 D23 (Fig. 3) is from a  $\sim 800 \text{ nm}$  diameter carbon grain with a  $^{14}\text{N}/^{15}\text{N}$  ratio of  $192 \pm 4$  ( $2\sigma$ ). Several  $^{15}\text{N}$ -enriched “hotspots” were identified in L2047 D23, although the measured bulk  $^{14}\text{N}/^{15}\text{N}$  ratio of the IDP ( $272 \pm 2$ ) is the same as the solar value ( $272$ ). L2036-C18-F4 (Fig. 3) is from a  $\sim 300 \text{ nm}$  diameter carbon grain with non-solar C and N isotopic compositions ( $^{12}\text{C}/^{13}\text{C} = 80 \pm 2.4$ ,  $^{14}\text{N}/^{15}\text{N} = 135 \pm 6.4$ ). This IDP has a non-solar bulk N composition ( $^{14}\text{N}/^{15}\text{N} = 203$ ). L2036-c24-I3 (Fig. 5) is from a  $\sim 650 \text{ nm}$  diameter cluster of GEMS with non-solar O isotopic compositions ( $^{16}\text{O}/^{17}\text{O} = 2262$  &  $^{16}\text{O}/^{18}\text{O} = 403$ )<sup>15</sup>. The isotopic signatures clearly establish that the grains are of (presolar) interstellar origin.

## Discussion

Small ( $\sim 15 \text{ nm}$  diameter) graphite particles and PAHs have long been favored as the most likely carriers of the astronomical  $2175 \text{ \AA}$  feature. However, small graphite particles are conspicuously absent in the most primitive meteoritic materials (meteorites and IDPs) and there is no spectral evidence of their presence in the ISM. Interest in graphite has been driven to some extent by computational considerations because it is one of the few (carbonaceous) materials for which good laboratory optical constants are available<sup>1</sup>. PAHs are ubiquitous in primitive meteoritic materials and there is evidence of their presence as both gases and solids in the ISM<sup>1</sup>. Moreover, they encompass a wide variety of substituted and unsubstituted moieties that could explain the observed variation in the bandwidth of the  $2175 \text{ \AA}$  feature. Hydrogenated amorphous silicates have largely been abandoned as carriers of the  $2175 \text{ \AA}$  feature in part because of perceived abundance constraints and because hydrogenated amorphous silicate models are not well developed<sup>2,3</sup>.

Our measurements of *bone fide* interstellar grains represent a novel approach in the search for the carrier(s) of the astronomical  $2175 \text{ \AA}$  extinction feature. The grains, organic carbon and amorphous silicates, are usually closely associated with one another in most IDPs (e.g. Fig. 2) and there strong evidence that they are coupled in the ISM<sup>1</sup>. The average bulk carbon content of IDPs ( $\sim 12 \text{ wt. \%}$ ) is a factor of  $\sim 3$  higher than the carbonaceous chondrites<sup>20,32</sup>. Graphitic carbon is conspicuously absent in most IDPs. Instead, it is amorphous and it typically forms a matrix that contains embedded mineral grains (Fig. 2)<sup>29</sup>. As much as half of the carbon is organic, 10-25% of it aliphatic and

much of the remainder presumably aromatic (e.g. PAHs)<sup>19,20</sup>. Synchrotron XANES measurements indicate that ~10% of the carbon is bound as carbonyl (C=O)<sup>20</sup>. A significant fraction of the carbonyl is bound to aromatic chromophores because in some IDPs the mass of carbonyl exceeds that of aliphatic compounds<sup>20</sup>. Non-solar D/H, <sup>13</sup>C/<sup>12</sup>C, and <sup>15</sup>N/<sup>14</sup>N anomalies in IDPs are associated with the organics<sup>13-15,21</sup>. The carbon is similar to kerogens found in carbonaceous chondrites, although there are significant structural and molecular differences<sup>19,33,34</sup>.

The central wavelength of the carbon 5.7 eV feature is constant (Fig. 3), suggesting a relatively homogenous kerogen, although isotopically anomalous “hotspots” indicate significant molecular heterogeneity<sup>13-15,21</sup>. The bandwidth of the carbon (and GEMS) features are also constant but broader than the astronomical feature (Fig. 3 & 4). However, bandwidths are sensitive to the physical state of grains<sup>35-37</sup>. These grains are no longer free-floating in the ISM and the extent to which they have been modified during their ~4.5 Gyr post-ISM lifetimes is unknown. Best fits to the 2175 Å feature using computer modeling are obtained when much smaller (<15 nm diameter) grains are used<sup>1-3</sup>. The strength of the carbon 5.7 eV feature correlates with the O/C ratio (Fig. 3). IR spectroscopy indicates that carbonyl (C=O) is the O carrier (Fig. 4). Therefore, the 5.7 eV feature from the carbon grains is likely due to organic molecules (e.g. PAHs) with carbonyl functionality. VEELS measurements of unsubstituted and carbonyl-substituted PAHs pyrene and pentacene confirm that the 5.7 eV feature is related to carbonyl functionality associated with aromatic chromophores. Carbonyl compounds have been detected in interstellar ices and they have also been synthesized in the laboratory when PAH/ice mixtures are exposed to proton and UV irradiation under simulated ISM conditions<sup>1,38,39</sup>.

GEMS contain at least two components that may contribute to the 5.7 eV feature. First, in addition to being coated with carbon, acid dissolution experiments suggest that some of them contain carbon within their interiors<sup>40</sup>. Second, the glassy matrices of GEMS are composed of hydroxylated amorphous magnesium silicates. Stoichiometric excesses of O observed in GEMS are due to hydroxyl ions (OH<sup>-</sup>) within their amorphous magnesium silicate matrices<sup>17,22</sup>. Steel and Duley (1987)<sup>6</sup> showed that laboratory UV spectra of hydroxylated amorphous magnesium silicate particles exhibit an absorption feature at 2175 Å, due to an electronic transition of hydroxyl ions in low-coordination sites (OH<sub>LC</sub><sup>-</sup>), that matches both the central wavelength and bandwidth of the interstellar feature (Figs. 1a-1c). In irradiated talc (Mg<sub>3</sub>Si<sub>4</sub>O<sub>10</sub>[OH]<sub>2</sub>) the feature is likely also due to OH<sub>LC</sub><sup>-</sup> because the intensity of feature increases with radiation damage (amorphization). Similarly, most of the hydroxyl in GEMS is probably OH<sub>LC</sub><sup>-</sup> because the glassy matrices are defect-rich from chronic exposure to irradiation in space<sup>17</sup>. The strong correlation between the 5.7 eV feature and O<sub>ex</sub> indicates that OH<sup>-</sup> is the dominant contributor in GEMS (Fig. 3a). It is not surprising that interstellar amorphous silicates exposed to irradiation are carriers of a 5.7 eV (2175 Å) feature since, in addition to OH<sub>LC</sub><sup>-</sup>, a variety of electronic transitions are possible in the 5-8 eV range in defect-rich amorphous silicas<sup>41</sup>.

## Summary

Interstellar carbon and amorphous silicate grains exhibiting a 5.7 eV (2175 Å) UV feature have been identified in chondritic IDPs collected in the stratosphere. The species responsible for the feature are carbonyl-containing organic compounds (probably PAHs) and hydrogenated amorphous silicates, both of which may have been produced by irradiation processing of dust in the ISM. Prior to this study carbonyl compounds were not implicated as carriers of the astronomical 2175 Å extinction feature, whereas amorphous silicates have been implicated. Identification of these carriers in *bone fide* interstellar grains provides new input for computational modeling, laboratory syntheses of grain analogues, and laboratory (UV) photo absorption measurements. Two carriers may explain the constant wavelength and variable bandwidth of the astronomical feature, with the relative abundance or state of each varying from one sightline to another. We cannot conclude that organic carbon and (hydroxylated) amorphous silicates are the *only* carriers of the astronomical feature. A variety of other carriers have been proposed including graphite “onions”, nano-diamonds, desiccated micro-organisms<sup>1-3</sup>, and even fullerenes that were discovered while attempting to synthesize the carrier of the interstellar 2175 Å feature<sup>42</sup>. However, organic carbon and amorphous silicates are the “common stuff” of interstellar space and cosmically abundant carriers are needed to explain the ubiquity of the 2175 Å feature.

## Methods

### Specimen preparation

Powder standards of talc, pyrene (C<sub>16</sub>H<sub>10</sub>), and 1-pyrene carboxaldehyde (C<sub>17</sub>H<sub>11</sub>O) were dispersed onto holey-carbon support films on 3 mm diameter Cu transmission electron microscope (TEM) grids. One chondritic IDP (W7013E17) was thin-sectioned using ultramicrotomy and transferred to a TEM grid. Four IDPs (L2047D23, L2036-c18-F4, L2036-C24-I3, and L2036 D16), were pressed into high purity gold foils for isotopic analyses using a NanoSIMS ion microprobe (see below). After the isotope measurements electron transparent sections (<100 nm thick) of the IDPs pressed into Au were extracted using a focused ion beam (FIB) technique<sup>43</sup>. The sections of L2036-D16 were transferred to holey carbon substrates where they were positioned over a hole in the carbon. (Carbon support substrates potentially interfere with the analyses because they produce a broad, weak feature at ~6.3 eV (Fig. 3). Extracted sections of L2047D23 and W7027 E17 were spot-welded to the edge of a Mo TEM grid using Pt.

### Transmission electron microscopy

High energy-resolution VEELS was carried out in combination with Z-contrast imaging using a FEI Tecnai G2 F20 UT (scanning) transmission electron microscope operating at 200 kV. The G2 is equipped with a high-resolution electron energy-loss spectrometer and a double-focusing Wien filter acting as a monochromator below the field-emission gun<sup>44,45</sup>. This electron optical configuration delivers a ~1 nm sized electron probe with an energy resolution of 0.18 eV. Acquisition times are typically between 0.5 and 1 s, for core losses between 3 and 10 eV.

For measurements of the 5.7 eV feature (Figs 3 & 4) we used the following settings: acquisition time: 1 s, dispersion: 0.02 eV/channel, monochromator potential: 800 V, monochromator excitation: 0.3, Spot size: 11, collection angle (VEELS): 5.6 mrad, convergence angle (monochromated electron probe): 20.6 mrad. In order to accurately scale the energy loss in the VEELS spectra, immediately after recording the valence "region" (down to ~0.5 eV) without the zero-loss peak, the spectrum was shifted by 1 eV and the zero-loss peak was recorded using a shorter acquisition time of 0.01 s.

The compositions of carbon and GEMS were measured in a 300 keV Philips CM300 field emission TEM equipped with an Oxford Instruments solid-state energy-dispersive x-ray (EDX) spectrometer and EmiSPEC spectral processing software. Spectra were quantified using an x-ray thin-film correction procedure. The precision and accuracy of the correction procedures were verified using NIST thin-film standard SRM2063 and by *in-situ* analyses of mineral grains of known compositions within the IDP sections.

### **Infrared spectroscopy**

The TEM specimen of IDP L2036 G16 was analyzed in transmission mode using an infrared microscope at the Advanced Light Source, Lawrence Berkeley National laboratory (beamline 1.4.3). The beamline is equipped with a ThermoNicolet Magna 760 FTIR bench and a SpectraTech Nic-Plan IR microscope. An MCT-A detector and KBr beamsplitter were used for mid-IR microspectroscopy. The synchrotron source was focused to a diffraction-limited 3-10  $\mu\text{m}$  diameter spot size onto the sample. The data was obtained by mapping the sample in 2 $\mu\text{m}$  steps and collecting spectra over 650 to 8000  $\text{cm}^{-1}$  wavelength range with 4  $\text{cm}^{-1}$  spectral resolution and 1026 sec dwell time. Spectra were normalized to the background spectrum collected over a hole in the substrate. Spectra are background subtracted and smoothed.

### **NanoSIMS Analyses**

IDP L2047D23 was analyzed with the Lawrence Livermore National Laboratory NanoSIMS 50 ion microprobe and IDPs L2036-c18-F4, L2036-C24-I3, and L2036-G16 were analyzed with the Washington University NanoSIMS 50<sup>14,15,28</sup>. The samples were pressed flat into high purity (99.999%) gold foil. Isotopic measurements were made with a ~1.5 pA, 16 keV  $^{133}\text{Cs}^+$  primary ion beam focused into a 100-150 nm diameter spot, rastered over sample areas ranging in size from 10 x 10 microns to 30 x 30 microns. The isotope imaging measurements consist of up to 40 replicate scans (layers) of 256 x 256 or 512 x 512 pixels with dwell times ranging from 1-10 ms/pixel. Secondary ion intensities were collected simultaneously in multi-collection mode using 3 different collector configurations, [ $^{16}\text{O}^-$ ,  $^{17}\text{O}^-$ ,  $^{18}\text{O}^-$ ,  $^{12}\text{C}^{14}\text{N}^-$ ,  $^{12}\text{C}^{15}\text{N}^-$ ], [ $^{12}\text{C}^-$ ,  $^{13}\text{C}^-$ ,  $^{12}\text{C}^{14}\text{N}^-$ ,  $^{12}\text{C}^{15}\text{N}^-$ ,  $^{28}\text{Si}^-$ ], and [ $^{16}\text{O}^-$ ,  $^{17}\text{O}^-$ ,  $^{18}\text{O}^-$ ,  $^{28}\text{Si}^-$ ,  $^{24}\text{Mg}^{16}\text{O}^-$ ]; secondary electron images were also recorded. A mass resolving power of ~6500 was used to separate isobaric interferences from the isotopes of interest, e.g.,  $^{16}\text{O}^1\text{H}$  from  $^{17}\text{O}$  at mass 17,  $^{13}\text{C}_2$  from  $^{12}\text{C}^{14}\text{N}$  at mass 26, and  $^{12}\text{C}^{15}\text{N}$  from  $^{13}\text{C}^{14}\text{N}$  at mass 27. The data were corrected for instrumental mass-dependent fractionation of C and N based on analyses of NIST SRM-8558 (potassium nitrate) mixed with NIST SRM-8541 (graphite) at LLNL and 1-hydroxy-benzotriazole-hydrate at Washington University; the magnitude of instrumental fractionation was generally <1%. Internal calibration was used for the O isotope imaging measurements.

The data were processed as quantitative isotopic ratio images using custom software that corrects for statistical outliers and image shift from layer to layer. Each analysis area was subdivided into region of interest (ROIs), and the isotopic composition for each ROI was calculated by averaging over all of the replicate layers. The compositions of isotopically anomalous ROIs were compared to similarly-sized regions of normal isotopic composition from the rest of the particle for an evaluation of the statistical significance of the anomalies. This approach identified several sub-micrometer size areas ('hotspots'), whose compositions in C, N, or O clearly indicate an interstellar (presolar) origin. The average isotope composition for whole IDPs was calculated as the weighted mean of the individual ROI values.

## References

1. Sandford, S. A. The inventory of interstellar materials available for the formation of the solar system. *Met. Planet. Sci.* **31**, 449-476 (1996).
2. Mathis, J. A. Observations and theories of interstellar dust. *Rep. Prog. Phys.* **56**, 605-652 (1993).
3. Draine, B. T. Interstellar dust grains. *Ann. Rev. Astron. Astrophys.* **41**, 241-289 (2003).
4. Stecher, T. P. Interstellar extinction in the ultraviolet. II *Ap. J.* **157**, L125-L126 (1969).
5. Carnochan, D. J. The variation of interstellar extinction in the ultraviolet. *Mon. Not. R. Astr. Soc.* **219**, 903-926 (1986).
6. Steel, T. M. and Duley, W. W. A 217.5 nanometer absorption feature in the spectrum of small silicate particles. *Ap. J.* **315**, 337-339 (1987).
7. Rietmeijer, F. J. M. In *Reviews in Mineralogy Vol. 36, Planetary Materials* (ed. Papike, J. J. ) 2-1 – 2-95 (Mineralogical Society of America, 1998).
8. Bradley, J. P. In *Treatise of Geochemistry* (eds. Davis, A. M., Holland H. D. & Turekian, K. K.) Vol. 1 689-711 (Elsevier, Amsterdam, 2004).
9. Bradley, J. P. and Brownlee, D. E. Cometary particles: thin sectioning and electron beam analysis. *Science* **231**, 1542-1544 (1986).
10. Bradley, J.P. and Brownlee D.E. An interplanetary dust particle linked directly to type CM meteorites and an asteroidal origin. *Science* **251**, 549-552 (1992).
11. Brownlee, D. E., Joswiak, D. J., Schlutter, D. J., Pepin, R. O., Bradley, J. P., & Love, S. J. Identification of individual cometary IDPs by thermally stepped He release. *Lunar Planet Sci.* **XXVI**, 183-184 (1995).
12. Schramm, L. S., Brownlee, D. E. and Wheelock, M. M. Major element composition of stratospheric micrometeorites, *Meteoritics* **24**, 99-112 (1989).
13. Messenger, S. (2000) Identification of molecular-cloud material in interplanetary dust particles. *Nature* **404**, 968-971 (2000).
14. Floss, C., Stadermann, F. J., Bradley, J. P., Dai, Z. , Bajt, S. and Graham, G. Carbon and nitrogen anomalies in an anhydrous interplanetary dust particle. *Science* **303**, 1355-1358 (2004).

15. Floss, C. and Stadermann, F. Isotopically Primitive Interplanetary Dust Particles of Cometary Origin: Evidence from Nitrogen Isotopic Compositions, *Lunar Planet Sci XXXV*, Abs. # 1281 (2004).
16. Messenger, S., Keller, L. P., Stadermann, F., Walker, R. M. and Zinner, E. (2003) Samples of stars beyond the solar system: silicate grains in interplanetary dust particles. *Science* **300**, 105-108.
17. Bradley, J. P. Chemically anomalous, preaccretionally irradiated grains in interplanetary dust from comets. *Science* **265**, 925-929 (1994).
18. Bradley, J. P., Keller, L. P., Snow, T. P., Hanner, M. S., Flynn, G. J., Gezo, J. C., Clemett, S. J., Brownlee, D. E. and Bowey, J. E. An infrared spectral match between GEMS and interstellar grains. *Science* **285**, 1716-1718 (1999).
19. Clemett, S. J., Maechling, C. R., Zare, R. N., Swan, P. D. and Walker, R. M. (1993) Identification of complex aromatic molecules in individual; interplanetary dust particles, *Science* **262**, 721-725.
20. Flynn, G. J., Keller, L. P., Jacobsen, C. and Wirrick, S (2003) An assessment of the amount and types of organic matter contributed to the Earth by interplanetary dust. *Adv. Space. Res.* **33**, 57-66.
21. McKeegan, K. D., Zinner, E. and Walker, R. M. (1985) Ion microprobe isotopic measurements of individual interplanetary dust particles. *Geochim. Cosmochim. Acta* **49**, 1971-1987.
22. Bradley, J. P., Dai, Z., Erni, R. and Browning, N. An analytical SuperSTEM for extraterrestrial materials research. *Lunar Planet. Sci.* **XXXV**, Abs. # 1433 (2004).
23. Stadermann, F. J. , Walker, R. M. and Zinner, E. Submicron isotopic measurements with the CAMECA NanoSIMS. *Lunar Planet. Sci.* **XXX**, Abs. # 1407 (1999).
24. Van Benthem, K. and Elsässer, C. and French, R. H. Bulk electronic structure of SrTiO<sub>3</sub>: experiment and theory. *J. Appl. Phys.* **90**, 6156-6164.
25. Dorneich, A. D., French, R. H., Müllejans, H., Loughin, S. and Rühle, M. Quantitative analysis of valence energy-loss spectra of aluminum nitride. *J. Microsc.* **191**, 286-296 (1998).
26. Gezo, J. C., Bradley, J. P. Brownlee, D. E., Kaleida, K. and Keller, L. P. Ultraviolet spectroscopy of interplanetary dust particles. *Lunar Planet Sci.* **XXXI**, Abs # 1816 (2000).

27. Brion, C.E., Daviel, S., Sodhi, R. & Hitchcock, A.P. Recent advances in inner-shell excitation of free molecules by electron energy loss spectroscopy. pp 429-446 in AIP Conference Proceedings No. 94: X-ray and atomic inner-shell physics-1982. Edited by Bernd Crasemann, American Institute of Physics, New York (1982).
28. Mason, N.J., Gingell, J.M., Jones, N.C. & Kaminski, L. Experimental studies on electron scattering from atoms and molecules: the state of the art. *Phil. Trans. R. Soc. Lond. A* **357**, 1175-1200 (1999).
29. Keller, L. P., Messenger, S. and Bradley, J. P. (2000) Analysis of a deuterium-rich interplanetary dust particle (IDP) and implications for presolar material in IDPs. *J. Geophys. Res.* **105** (A5), 10397-10402.
30. Sandford, S. A. , Allamandola, L. L., Tielens, A. G. G. M., Sellgren, K., Tapia, M., and Pendelton, Y. The interstellar C-H stretching band near 3.4 microns: Constraints on the composition of organic material in the diffuse interstellar medium. *Ap. J.* **371**, 607-620 (1991).
31. Keller, L. P., Messenger, S., Flynn, G. J., Clemett, S., Wirick, S. and Jacobsen, C. The nature of molecular cloud material in interplanetary dust. *Geochim. Cosmochim. Acta* **68**, 2577-2589 (2004).
32. Keller, L. P, Thomas, K. L. and McKay, D. S. Carbon in primitive interplanetary dust particles. In *Analysis of interplanetary dust* (eds. M. E. Zolensky, T. L. Wilson, F. J. M. Rietmeijer, G. J. Flynn), pp. 51-87. (AIP Conf. Proc. 310, Am. Inst. Phys. New York, 1994).
33. Wopenka, B. Raman observations of individual interplanetary dust particles. *Earth Planet. Sci. Lett.* **88**, 221-231 (1988).
34. Quirico, E., Borg, J., Raynal, P-I and d'Hendecourt, L. A micro-raman study of 10 IDPs and 6 carbonaceous chondrites. *Lunar Planet. Sci.* XXXV, Abs # 1815 (2004).
35. Ehrenfreund, P., D'Hendecourt, L., Verstraete, Leger, A. Schmidt, W. and Defourneau, D. Search for the 4430 Å DIB in the spectra of coronene cation and neutral ovalene. *Aston. Astrophys.* **259**, 257-264 (1992).
36. Schnaiter, M., Mutschke, H., Dorschner, J. and Henning, Th. Matrix-isolated nano-sized carbon grains as an analog for the 217.5 nm feature carrier. *Ap. J.* **498**, 286-406 (1998).
37. Rouleau, F., Henning, Th. And Stognienko, R. Constraints on the properties of the 2175 Å interstellar carrier feature. *Astron. Astrophys.* 322, 633-645 (1997).

38. Bernstein, M. P., Moore, M. L., Elsila, J. E., Sandford, S. A., Allamandola, L. J. and Zare, R. N. Side group addition to the polycyclic aromatic hydrocarbon coronene by proton irradiation in cosmic ice analogs. *Ap. J.* **582**, L25-L29 (2003).
39. Bernstein, M. P., Sandford, S. A., Allamandola, L. J., Gillette, J. S., Clemett, S. J., & Zare, R. N. UV Irradiation of Polycyclic Aromatic Hydrocarbons in Ices: Production of Alcohols, Quinones, and Ethers. *Science* **283**, 1135-1138 (1999).
40. Brownlee, D. E., Joswiak, D. J., Bradley, J. P., Gezo, J. C., and Hill, H. G. M. Spatially resolved acid dissolution of IDPs: the state of carbon and the abundance of diamonds in the dust. *Lunar planet. Sci.* **XXXI**, 1921-1922 (2000).
41. O'Reilly, E. P. and Robertson, J. Theory of defects in vitreous silicon dioxide. *Phys. Rev. B* **27**, 3780-3795 (1983).
42. Kroto, H. W., Heath, J. R., O'Brien, S. C., Curl, R. F. and Smalley, R. E. C(60): Buckminsterfullerene. *Nature* **318**, 162-163 (1985).
43. Graham, G. A., Bradley, J. P., Bernas, M., Stroud, R. M., Dai, Z. R., Floss, C., Stadermann, F. J., Snead, C. J. and Westphal, A. J. Focused ion beam recovery and analysis of interplanetary dust particles (IDPs) and Stardust analogues. *Lunar Planet. Sci.* **XXXV**, Abs. #2044 (2004).
44. Brink, H.A., M.M.G. Barfels, Burgner, R.P. & Edwards, B.N. A sub-50 meV spectrometer and energy filter for use in combination with 200 kV monochromated (S)TEMs. *Ultramicroscopy* **96**, 367-384 (2003).
45. Tiemeijer, P.C. Measurement of Coulomb interactions in an electron beam monochromator. *Ultramicroscopy* **78**, 53-62 (1999).

## **Acknowledgement**

This research is supported by NASA grants and NAG5-10632 (JPB) and NAG5-10696 10696 (JPB) and NNG04GG49G (CF, FJS). The research was also in part performed under the auspices of the U.S. Department of Energy, National Nuclear Security Administration by the University of California, Lawrence Livermore National Laboratory under contract No. W-7405-Eng-48. Electron microscopy performed at the National Center for Electron Microscopy at Lawrence Berkeley National Laboratory (LBNL) supported by DoE contract No. DE-AC03-76SF000098. We thank L. Nittler for image processing software development. We gratefully acknowledge discussions with M. Bernstein, D. Brownlee, B. Draine, Th. Henning, X. Tielens and Farid Salama.

## Figure Captions

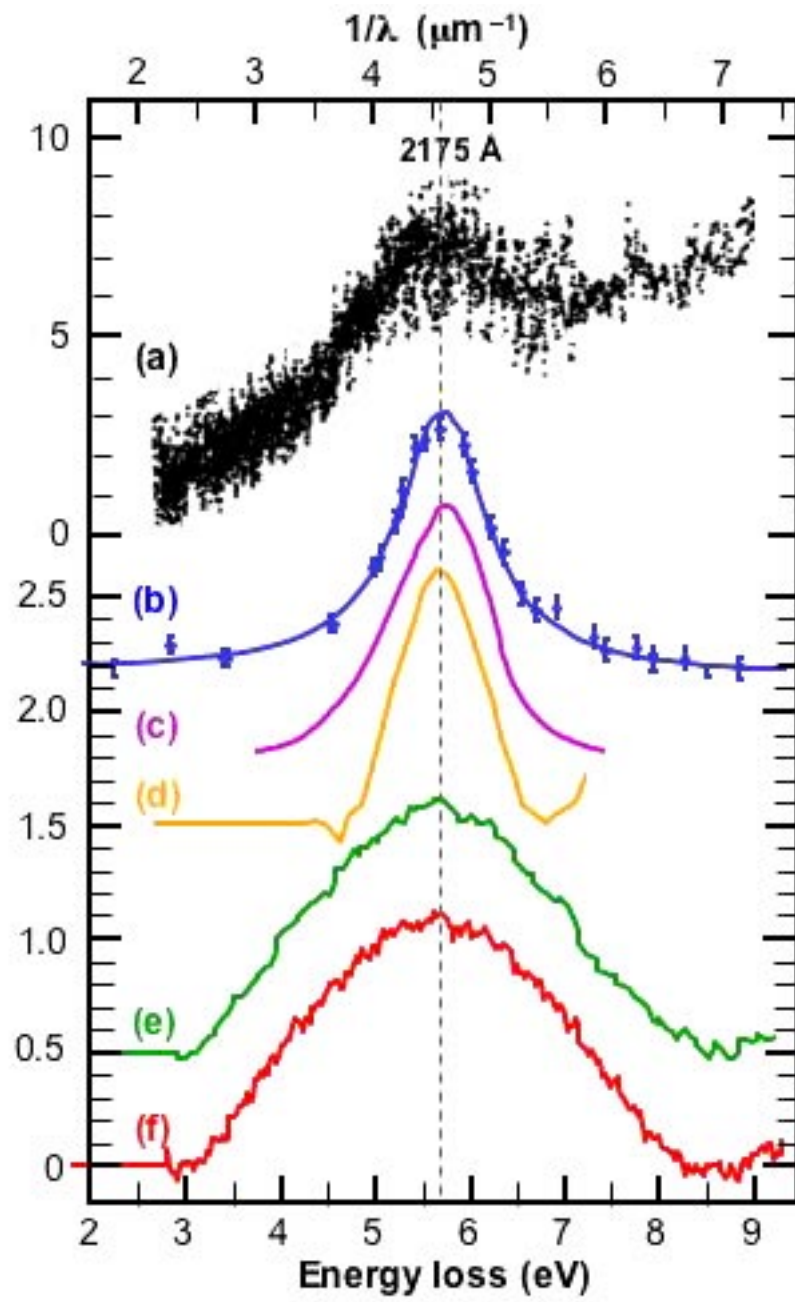
Figure 1. Comparison of astronomical UV extinction features with laboratory UV and VEELS features. (a) The 2175 Å interstellar extinction feature from two stars ζ and ε Persei<sup>4</sup>. (b) The profile as derived from 13 stars. Continuous line is the best fit Lorentzian<sup>5</sup>. (c) Photo-absorption spectrum from partially-recrystallized hydroxylated amorphous magnesium silicate ( $\text{Mg}_2\text{SiO}_4[\text{OH}]_n$ )<sup>6</sup>. (d) VEELS spectrum from (electron) irradiation damaged talc ( $\text{Mg}_3\text{Si}_4\text{O}_{10}[\text{OH}]_2$ ). (e) VEELS spectrum from (organic) carbon in IDP L2047 D23. (f) VEELS spectrum from GEMS in W7013 E17. Vertical scale in (a) is magnitude, and in (b) through (f) normalized logarithmic.

Figure 2. 200 keV brightfield transmission electron micrograph of carbon (C) and GEMS within chondritic interplanetary dust particle L2009\*E2.

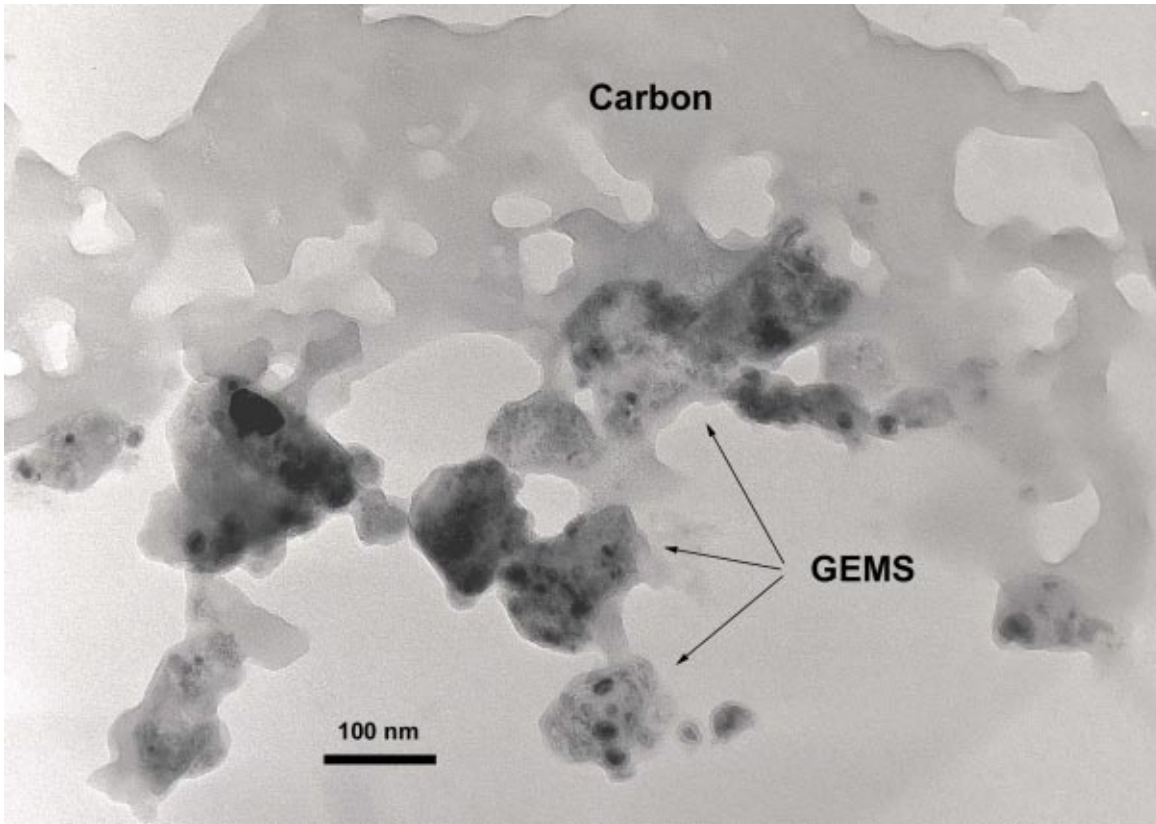
Figure 3. VEELS spectra from carbon: (a) L2036-G16, (b) L2047 D23, (c) L2036-C18-F4, (d) amorphous carbon film. O/C is element ratio of oxygen to carbon.

Figure 4 (a) Infrared spectrum from a ~3X3 μm region of carbon in IDP L2036 G16 (see also Fig. 3a). Peaks 2850-2960  $\text{cm}^{-1}$  are due to aliphatic C-H stretch modes and the peak at ~1720  $\text{cm}^{-1}$  is due to carbonyl (C=O). Specimen thickness is <100 nm. Insets (a) & (b), 300 keV electron energy-loss spectra (monochromator off) of carbon-K edge showing double  $\pi^*$  edges (dashed lines) at ~285.0 eV and 286.5 eV consistent with carbonyl (C=O)<sup>20</sup>, and oxygen-K edge showing a pre-edge at ~531 eV (arrowed) associated with a  $1s$  to  $\pi^*$  transition of oxygen and also consistent with carbonyl<sup>20</sup>.

Figure 5. VEELS spectra from GEMS (a)-(c) W7013E17 ( 3 GEMS), (d) L2036-C24-I3, (e) L2036-C18-F4.  $\text{O}_{\text{ex}}$  is hydroxyl (-OH) as excess oxygen over stoichiometry<sup>16,27</sup>. The feature at 10.5 eV is an exciton characteristic of silicates.



**Figure 1**



**Figure 2**

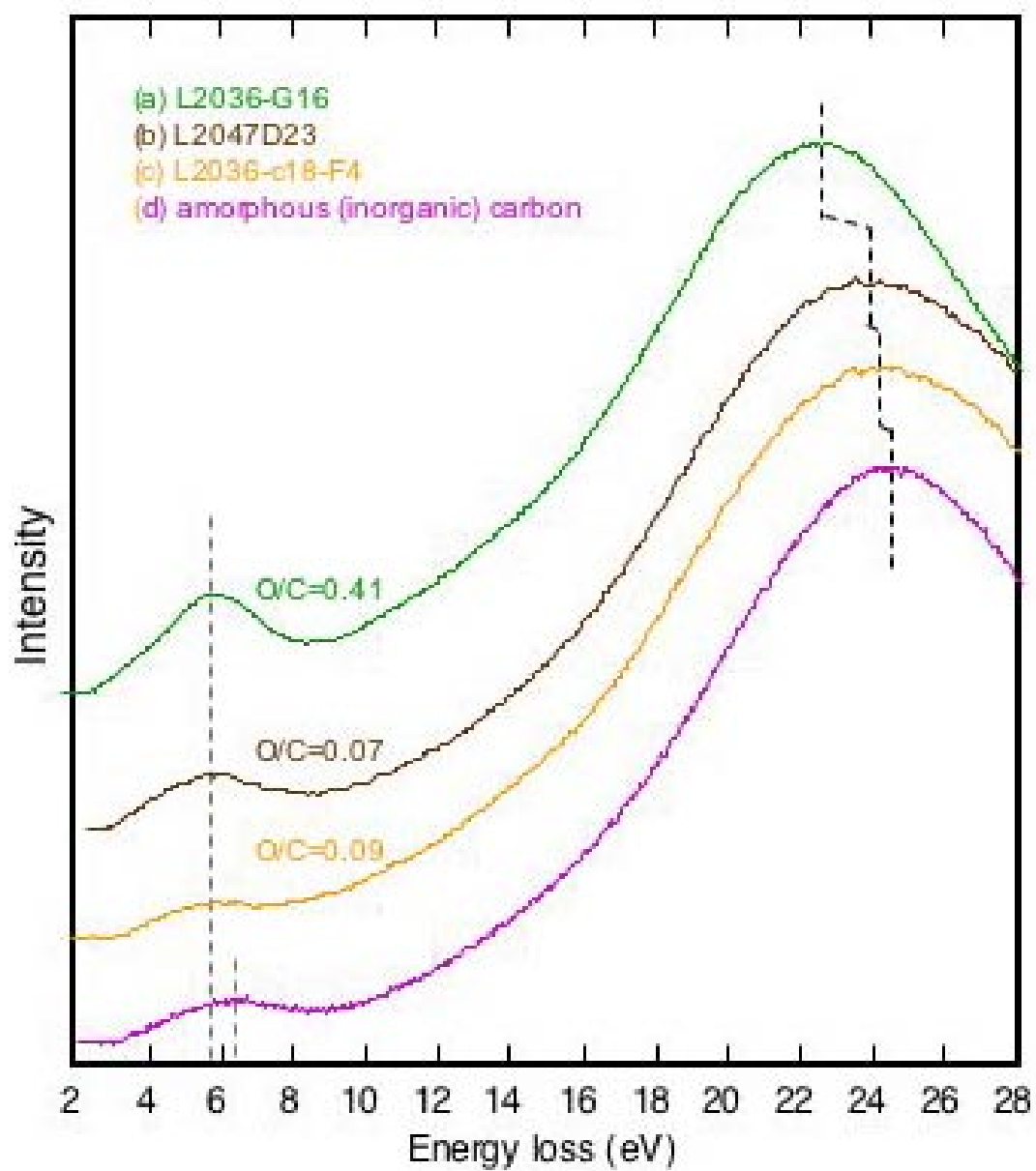


**Figure 3**

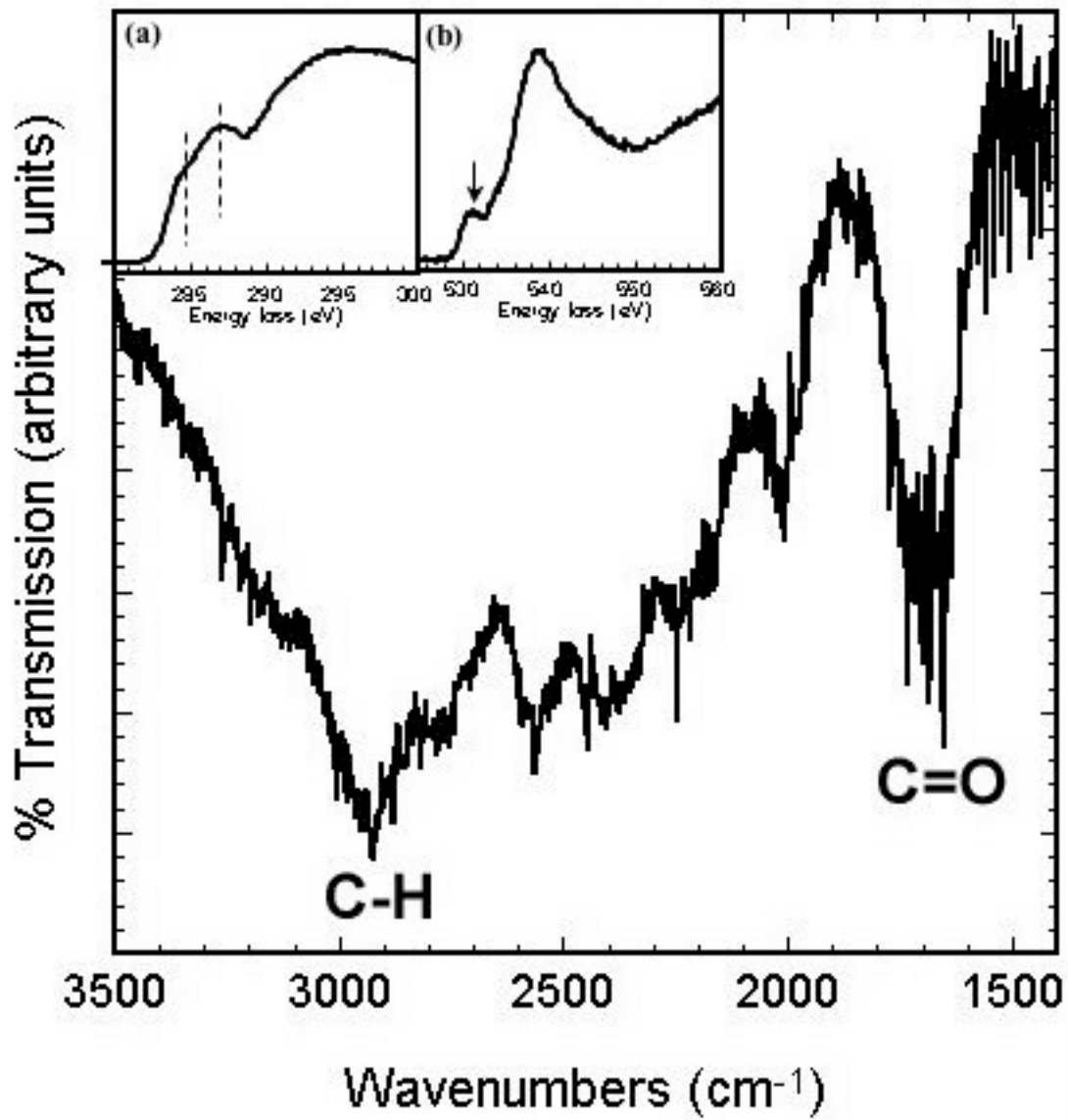
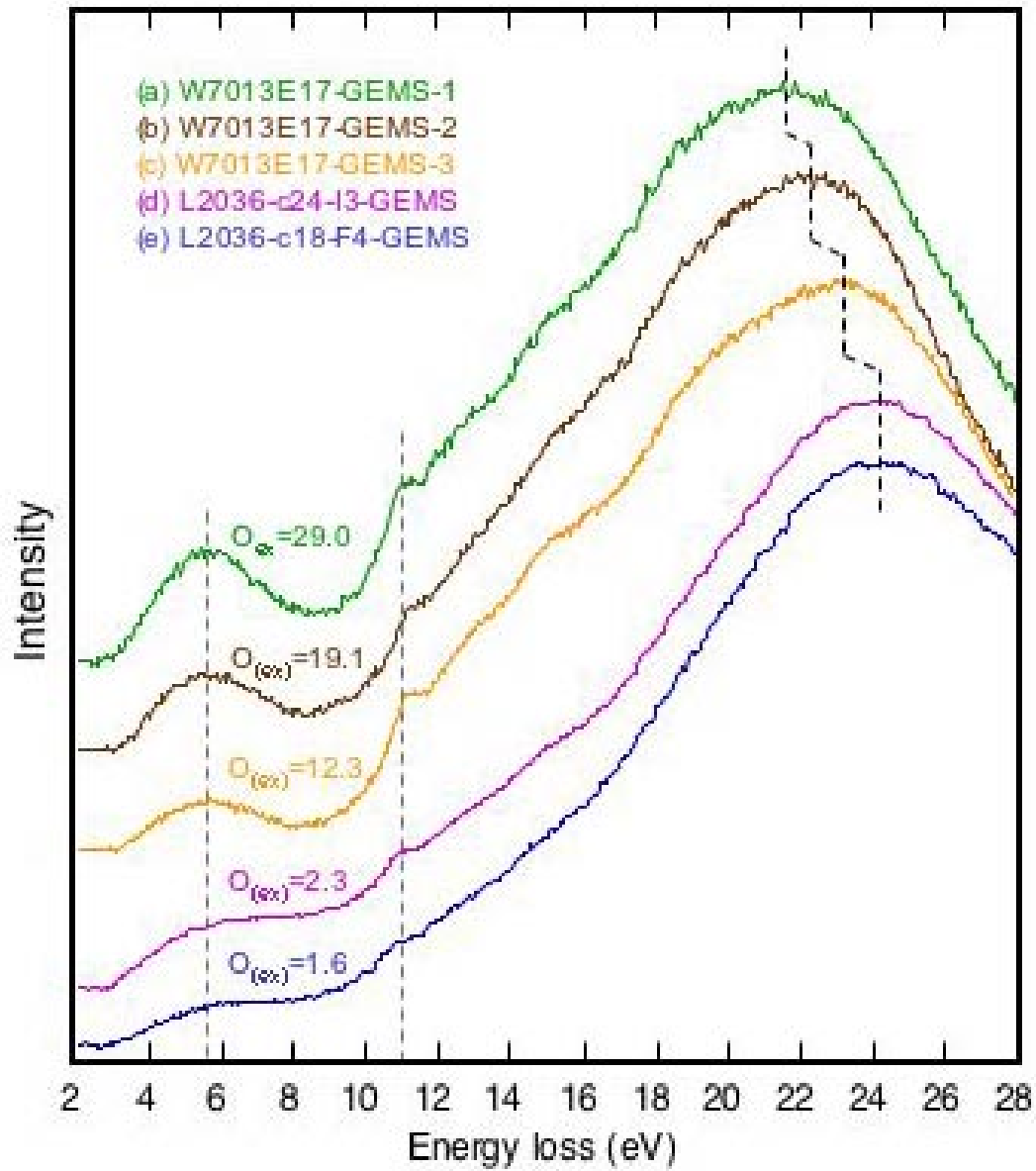


Figure 4



**Figure 5**